

Net Charge Accretion in Magnetized Kerr Black Holes

Ethan Berreby,^{1,*} Avner Okun,^{1,†} Shahar Hadar,^{2,3,‡} and Amos Ori^{1,§}

¹*Department of Physics, Technion, Haifa 32000, Israel*

²*Department of Mathematics and Physics, University of Haifa at Oranim, Kiryat Tivon 3600600, Israel*

³*Haifa Research Center for Theoretical Physics and Astrophysics, University of Haifa, Haifa 3498838, Israel*

We investigate the charging process of a rotating Kerr black hole of mass M and angular momentum J immersed in a stationary, axisymmetric, asymptotically uniform magnetic field of strength B_0 . In Wald's classic analysis [1], which was based on the assumption of vanishing injection energy, the black hole was predicted to acquire a universal "saturation charge" $Q_w = 2B_0J$. However, the physical mechanism that sets the saturation charge must ultimately be governed by the competition between the absorption rates of positively and negatively charged particles. Motivated by this observation, we revisit the problem in the framework of a simple accretion model, where two dilute, equivalent fluxes of charged particles of opposite signs are injected from infinity along the magnetic field lines. The problem then reduces to that of individual particle motion in the electromagnetic field of the magnetized Kerr black hole. Using a combination of numerical and analytical tools, we determine the domains of absorption and establish both lower and upper bounds on the corresponding absorption cross sections. At $Q = Q_w$ these bounds reveal a systematic difference between the two charge signs. In particular, for sufficiently strong magnetic fields, the lower bound on the absorption cross section for the "attracted" charge exceeds the upper bound for the "repelled" one. This charge accretion imbalance (which we find to become extreme at the limit of large B_0) indicates a persistent net charge accretion at $Q = Q_w$, implying that the actual saturation charge must differ from Wald's charge Q_w .

I. INTRODUCTION

When a rotating black hole (BH) is immersed in an environmental magnetic field, the strong curvature distorts the electromagnetic field, creating an electric field – which may be strong in the close vicinity of the BH. Such an induced electric field may potentially lead to various astrophysical effects [2–4].

About half a century ago, Wald investigated the case of a Kerr BH immersed in an asymptotically uniform magnetic field aligned with the BH's axis of rotation (where the electromagnetic field is assumed to be too small to affect the background metric) [1]. He found that in this case, a (current-free) four potential $A_\mu(x)$ can be directly constructed from the two Killing fields of the Kerr background. This construction leads to a two-parameter family of solutions to Maxwell's equations. The first parameter is the asymptotic magnetic field magnitude B_0 , and the second parameter, Q , is the BH's charge.

An inspection of the $Q = 0$ case of Wald's solution for $A_\mu(x)$ shows that along the symmetry axis, there is a non-vanishing, radially directed, electric field. As a consequence, in an astrophysical environment that contains free charged particles, the electric field at the pole will selectively attract charges of one sign over the other, leading one to anticipate a non-vanishing net charge accretion. In turn, this net current will cause Q to gradually drift away from zero, eventually reaching a certain

saturation charge $Q_{\text{sat}} \neq 0$.

In his paper [1], Wald also investigated the expected value of the saturation charge under the assumption that the so-called injection energy of charged particles into the BH should vanish at $Q = Q_{\text{sat}}$. This assumption led to a simple, universal value for the saturation charge $Q_{\text{sat}} = 2B_0J \equiv Q_w$ where J denotes the BH's angular momentum. As a technical remark, note that Q_w is positive if the BH's angular momentum and the asymptotic magnetic field are co-directed, and negative otherwise. Throughout this paper, without loss of generality, we shall assume that $Q_w > 0$. Correspondingly, we shall often refer to negatively charged particles as *attracted* and to positively charged ones as *repelled*, which will be denoted with superscripts "–" and "+" respectively.

We are not convinced, however, that the concept of injection energy can dictate the actual value of the saturation charge. Obviously, the saturation charge should be determined by the absorption rates for both the positively and negatively charged particles. To our understanding, the phenomenon of absorption of a particle by a BH (which is key to the determination of the absorption cross sections and hence, absorption rates) is a dynamical process, not one governed by equilibrium considerations.

The problem of charge accretion into a magnetized Kerr BH has previously been considered in [5] (under the simplifying assumption that charged particles move along the magnetic field lines, even in the BH's vicinity). Their results seem to differ from Wald's picture in several respects. In particular, the authors contemplate the possibility that the BH charge oscillates rather than approaches a steady state. Another question mark regarding Wald's picture was raised in [6] where it was suggested that the system's total electromagnetic-field energy may

* ethanberreby@campus.technion.ac.il

† avnerok@campus.technion.ac.il

‡ shaharhadar@sci.haifa.ac.il

§ amos@physics.technion.ac.il

be a more relevant criterion than the injection energy of individual charges. The charge that minimizes the total electromagnetic energy is found there to differ from Wald's charge. In addition, although the system considered in [7] differs from the one analyzed by Wald (they consider a boosted magnetized BH), we find it relevant to mention the authors' viewpoint that detailed particle dynamics (rather than mere energetic arguments) should determine the BH's charge.

Motivated by the desire to better understand the saturation charge Q_{sat} , in this work we set out to develop an accretion model as natural and simple as possible, which will allow us to quantitatively explore the absorption rates in terms of the corresponding cross sections – and thereby, to determine whether there actually is charge accretion balance or imbalance at $Q = Q_w$. In our setup, there are two twin uniform fluxes of unbound positively and negatively charged particles coming from infinity along the magnetic field lines. These two fluxes are fully equivalent, in the sense that they share the same flux density, and the positive and negative charges have the same mass m , the same charge magnitude $|e|$, and the same asymptotic incoming velocity – they only differ by the sign of the particles' charge (a more detailed description of our accretion model is given in the next section). We assume that the fluxes are very dilute, such that individual charges do not affect each other's motion. In this situation, assuming equal fluxes, the issue of charge accretion balance (or imbalance) boils down to the question of whether the two absorption cross sections are equal or not – which is the question on which we focus throughout this paper.

Due to the symmetries of the electromagnetic field (and the Kerr metric), the particles' orbits admit two constants of motion: the energy E and the azimuthal angular momentum L . The energy E (> 1) is assumed to be the same for all particles composing the two fluxes. The angular momentum L is uniquely determined by the orbit's impact parameter b . Due to the presence of the electromagnetic field, Carter's constant is *not* conserved, and as a consequence, we are unable to solve the equations of motion (EOM) analytically. We therefore solve them numerically, with the aim of determining whether a given orbit falls into the BH or not. Our goal is to figure out, for each of the two charges (for a given set of the model's parameters M, J, B_0, E and the particles' charge-to-mass ratio $\frac{e}{m}$), what is the domain of absorption on the b axis – which, in turn, determines the absorption cross section σ .

Naively, one might expect to find a single continuous domain of absorption that extends from $b = 0$ up to a certain critical value \tilde{b} beyond which no orbit would be absorbed (in which case the cross section would be $\pi\tilde{b}^2$). Indeed, there is a central, continuous, absorption domain from $b = 0$ up to a certain value b_1 ; but to our surprise, we found that at $b > b_1$, the family of orbits has a fractal structure. In particular, in the range $b > b_1$, there appear to exist an infinite set of individual absorption (as well

as non-absorption) domains. We note that such a fractal behavior has been observed in magnetized Schwarzschild [8] and Kerr [3, 7] BHs. nevertheless, this fractal behavior has not been observed or analyzed so far in the context of a family of unbound orbits coming from infinity.

This fractal behavior makes it extremely challenging to precisely quantify the absorption cross sections. We therefore opted for a method of evaluating lower and upper bounds on these cross sections as we now explain. First, as mentioned above, there always exists a central absorption domain $0 \leq b < b_1$. Hence, by numerically finding this parameter b_1 , we obtain a lower bound on the accretion cross section $\sigma_{\min} = \pi(b_1)^2$. Second, with the help of the constants of motion, we construct an analytical criterion which tells us in which regions on the $r - \theta$ plane a particle can be present as a function of b (which determines L , as mentioned above). By analyzing this criterion, we obtain a certain value b_0 beyond which particles cannot reach the event horizon at all. This, in turn, gives us an upper bound on the cross section $\sigma_{\max} = \pi(b_0)^2$.

By comparing the lower bound for the attracted charge σ_{\min}^- with the upper bound for the repelled one σ_{\max}^+ , we find that for all values of BH spin and mass and every $E > 1$, at strong enough magnetic fields, $\sigma_{\min}^- > \sigma_{\max}^+$. This indicates that there is net accretion imbalance at $Q = Q_w$, as the absorption rate of attracted charges is larger than that of the repelled ones. In turn, this implies that the actual saturation charge must be smaller than Q_w . In fact, we find that at the limit of strong magnetic field, while σ_{\min}^- approaches a constant value of order a few times M^2 , σ_{\max}^+ approaches zero.

In order to investigate charge accretion imbalance, we proceed in two stages. We start by choosing a specific point in the space of our model's parameters – namely specific values of $\frac{J}{M^2}$, E and B_0 – for which the analysis becomes especially simple, and demonstrate imbalance in this specific case. Then, in the next stage, we extend the analysis to the entire range of B_0 and show that charge accretion imbalance is guaranteed to occur beyond a certain value of B_0 . Moreover, the “imbalance ratio” $\frac{\sigma^-}{\sigma^+}$ diverges at the limit of large B_0 ¹.

In Sec. II we review Wald's solution for $A_\mu(x)$ and use it in our accretion analysis. As already mentioned above, in our model a charged particle comes in from infinity along the magnetic field lines with a certain energy $E > 1$ and impact parameter b . Due to the scale invariance of general relativity, the relevant model's parameters reduce to the BH's specific spin $\alpha \equiv \frac{J}{M^2}$, the magnetic field strength parameter $\varepsilon \equiv \frac{e}{m}B_0M$, as well as E and b . We write down the particles' EOM, and relate the impact parameter b to the conserved angular momentum L .

¹As a matter of fact, the magnitude of the magnetic field will later be quantified by means of the dimensionless parameter ε defined below, rather than B_0 itself.

In Sec. III we investigate the various types of orbits and explore the structure of the trajectory space, by numerically solving the EOM for a variety of initial conditions. We distinguish between three types of orbits: those falling into the BH, those escaping to infinity, and orbits that stay trapped forever in the BH exterior. In our analysis, we focus on the central absorption domain $0 \leq b < b_1$ and numerically evaluate b_1 for a variety of parameters, providing a lower bound on the absorption cross section. In addition, we carefully take the $\varepsilon \rightarrow -\infty$ limit of the EOM, which exhibits significant simplification and thereby provides a valuable insight on the accretion behavior at large magnetic fields.

In Sec. IV we implement a complementary analytical approach based on the constants of motion E and L (as well as the normalization of the four-velocity). This method provides a simple analytical criterion telling us in which regions in the $r - \theta$ plane the particle is allowed to be present. For each value of b this criterion enables us to say whether or not the particle is allowed to be absorbed into the BH. In turn, this gives us an upper bound b_0 on the absorption range on the b axis – and hence an upper bound on the absorption cross section. To facilitate this analysis, we introduce the notion of *critical points* – points at which the topology of the allowed region changes – and show how their properties can be used to determine b_0 . For the repelled particle, our analysis also reveals the presence of an analytical upper bound $b_h \propto \varepsilon^{-\frac{1}{2}}$ on b_0 .

In Sec. V we compare the upper bound $\sigma_{\max}^+ = \pi(b_0^+)^2$ for repelled particles obtained using the conserved quantities based criterion with the numerically obtained lower bound $\sigma_{\min}^- = \pi(b_1^-)^2$ for attracted particles, and we demonstrate an imbalance in charge accretion.

In Sec. VI we discuss our results and their physical implications. In particular, the charge accretion imbalance demonstrated in Sec. V indicates that Wald's charge Q_w cannot be a universally valid saturation charge of a magnetized Kerr BH. We briefly mention our preliminary results for the anticipated correction to Wald's charge, that will be the focus of a forthcoming paper [9]. In particular, we find that Wald's charge remains the correct leading-order saturation charge in the limit of large $|\varepsilon|$. We also demonstrate that this case of large $|\varepsilon|$ is astrophysically relevant.

Rotating BHs in magnetized environments are believed to play a central role in a variety of observed astrophysical phenomena. The results in this paper shed new light on their charging mechanism (although only for situations of extremely dilute environments), and in particular refine our understanding of their steady-state charge. Throughout this paper we use relativistic units $G = c = 1$.

II. PRELIMINARIES

A. Wald solution

It has been shown by Wald [1] that the source-free vector potential induced by a stationary and axisymmetric Kerr BH, placed in an asymptotically uniform magnetic field which is asymptotically aligned with the axis of rotation, can be constructed using the timelike and axial Killing vectors $\eta^\mu \equiv g_t^\mu$ and $\psi^\mu \equiv g_\phi^\mu$ respectively, where $g_{\mu\nu}$ is the spacetime metric, and t and ϕ are respectively the standard temporal and azimuthal Boyer-Lindquist coordinates, see Eq. (5). Wald's potential is given by

$$A_\mu = \left(\frac{B_0 J}{M} - \frac{Q}{2M} \right) g_{t\mu} + \frac{1}{2} B_0 g_{\phi\mu}, \quad (1)$$

where M and J are respectively the mass and angular momentum of the BH, and B_0 is the magnetic field magnitude at infinity. The parameter Q is the charge of the BH, assumed to be too small to have an effect on the metric².

It is evident from (1) that a nontrivial electric potential is created in the vicinity of the BH. If the BH is surrounded by charged particles (or plasma), as is often the case in various astrophysical scenarios, the existence of this electric potential suggests that selective accretion of charge will take place, leading to a non-vanishing net charge accretion. This net current gradually modifies the BH's charge Q until the latter arrives at a *saturation value* at which the net charge accretion vanishes. Wald suggested that this saturation charge takes the universal value $Q_w = 2B_0 J$. This is the special charge value at which the electric field vanishes everywhere along the symmetry axis $\theta = 0$ (leading to a vanishing injection energy [1]).

In this paper we analyze the proposed steady state situation $Q = Q_w$ in more detail by analyzing the rate of charge accretion for charges of both signs, considering the full EOM of a charged test particle in such a system. It is important to note that this model is applicable only in situations where the interactions between infalling charges are negligible. Otherwise, the system may transition from vacuum to plasma dynamics, and the present analysis is no longer applicable [3]. We then enter the realm of magnetohydrodynamics, which will not be considered in this paper.

In this paper, unless explicitly stated otherwise, we will choose our units such that the mass of the BH, M , is equal to 1 (in addition to $G = c = 1$). This allows us to rewrite the four-potential as

²The effect of the electromagnetic field (associated with the BH's charge Q) on the metric is expected to be negligible for known astrophysical examples (see [1]).

$$\frac{e}{m}A_\mu = \varepsilon \left(\alpha(1-\lambda)(g_{t\mu} + \delta_{t\mu}) + \frac{1}{2}g_{\phi\mu} \right), \quad (2)$$

where $\delta_{t\mu}$ denotes Kronecker's delta, m and e are the particle's mass and charge respectively, and we will refer to $\varepsilon \equiv \frac{e}{m}B_0M$ as the *dimensionless magnetic field strength*, $\alpha \equiv a/M$ is the *dimensionless spin parameter*, and $\lambda \equiv Q/Q_w$ is the charge in units of Q_w (We have chosen to present these quantities with a reintroduction of the BH mass to highlight that they remain dimensionless regardless of the choice of $M = 1$ units). In (2), we added the gauge term $\varepsilon\alpha(1-\lambda)\delta_{t\mu}$ such that the electric potential vanishes at infinity. Note that $\text{sign}(\varepsilon)$ depends on the charge of the infalling particle relative to the sign of Q_w . Correspondingly, we refer to the cases of $\text{sign}(\varepsilon) = +1, -1$ as *repelled/attracted* particles, respectively. The field strength is therefore

$$\frac{e}{m}F_{\mu\nu} = \varepsilon \left[\alpha(1-\lambda)(g_{t\nu,\mu} - g_{t\mu,\nu}) + \frac{1}{2}(g_{\phi\nu,\mu} - g_{\phi\mu,\nu}) \right]. \quad (3)$$

In order to study charge accretion at $Q = Q_w$, we will set $\lambda = 1$ unless stated otherwise.

B. Equations of motion

The EOM of a charged particle moving in an electromagnetic field are

$$\frac{du^\alpha}{d\tau} + \Gamma_{\mu\nu}^\alpha u^\mu u^\nu = \frac{e}{m}F^\alpha{}_\nu u^\nu, \quad (4)$$

where the four-velocity u^μ is also subject to the constraint $u^\mu u_\mu = -1$. Note that in this paper, we will not consider any self-force effects³.

Throughout this paper we assume that the particle is moving in the Kerr metric, given in Boyer-Lindquist coordinates (with M set to 1) by

$$ds^2 = -\left(1 - \frac{2r}{\Sigma}\right)dt^2 - \frac{4r\alpha \sin^2\theta}{\Sigma}dtd\phi + \frac{\Sigma}{\Delta}dr^2 + \Sigma d\theta^2 + \frac{(r^2 + \alpha^2)^2 - \Delta\alpha^2 \sin^2\theta}{\Sigma} \sin^2\theta d\phi^2, \quad (5)$$

where

$$\Sigma = r^2 + \alpha^2 \cos^2\theta, \quad \Delta = r^2 - 2r + \alpha^2. \quad (6)$$

The event horizon is located at the r value $r_+ \equiv 1 + \sqrt{1 - \alpha^2}$, which solves $\Delta = 0$.

Since both the metric and the electromagnetic potential are stationary and axisymmetric, there are two conserved quantities

$$E = -u_t - \frac{e}{m}A_t, \quad L = u_\phi + \frac{e}{m}A_\phi, \quad (7)$$

where E and L are respectively the energy and angular momentum of the particle per unit mass. These two quantities correspond to the t and ϕ components of the four-momentum of a charged particle in an electromagnetic field:

$$\frac{p_\mu}{m} = u_\mu + \frac{e}{m}A_\mu. \quad (8)$$

In this paper, we focus on the case of a BH set at Wald's charge, and correspondingly we take (2) with $\lambda = 1$ as the four-potential. As a consequence, the four-potential becomes

$$\frac{e}{m}A_\mu = \frac{1}{2}\varepsilon g_{\phi\mu}, \quad (9)$$

the field strength

$$\frac{e}{m}F_{\mu\nu} = \frac{1}{2}\varepsilon(g_{\phi\nu,\mu} - g_{\phi\mu,\nu}), \quad (10)$$

and the constants of motion E and L

$$E = -u_t - \frac{1}{2}\varepsilon g_{\phi t}, \quad (11)$$

$$L = u_\phi + \frac{1}{2}\varepsilon g_{\phi\phi}. \quad (12)$$

Due to the nonlinear nature of the EOM and the lack of a sufficient number of conserved quantities⁴, for generic orbital parameters these equations are analytically intractable, and a numerical approach must be implemented for their solution. Alternatively, one may use (semi-)analytical energy considerations. We shall use both of these approaches to derive lower and upper bounds on the absorption cross section for charged particles.

C. Defining the physical system

We consider the motion of test charged particles in the background of a Kerr BH immersed in an asymptotically uniform magnetic field, with A_μ corresponding to a

³Nevertheless, as will be mentioned below (see Subsec. II C), in our model we disregard any initial Larmor motion of incoming particles, and our motivation for this assumption is the radiative decay of any such cyclotron motion already before the particle has arrived in the vicinity of the BH.

⁴The electromagnetic field (1) breaks the symmetry responsible for the conservation of the Carter constant in Kerr [10].

Wald-charged BH, given by (9). We assume that all test charges come in from infinity. Far from the BH region, the particles are moving in a uniform magnetic field. The most general motion of a charged particle in such a uniform magnetic field proceeds along a certain fixed magnetic field line, with a cyclotron motion (also referred to as *Larmor motion*) characterized by a constant Larmor radius. Our model assumes that the incoming charges arrive from infinity with *zero Larmor radius*. The physical motivation for this assumption is simple: Since the charges arrive from infinity, any initial Larmor motion would be lost due to cyclotron radiation long before the charges approach the vicinity of the BH.

Each particle's trajectory is characterized by an impact parameter b (with respect to the symmetry axis $\theta = 0$). It is also characterized by its energy $E > 1$, which corresponds to a particle coming from infinity with asymptotic velocity > 0 . For given initial parameters E and b , we ask whether the particle is absorbed into the BH.

All particles are assumed to be of the same mass m and the same charge magnitude which is either $+e$ or $-e$. The (asymptotically uniform) influx of charges of both signs is assumed to be equal, and all particles have the same energy E . We are primarily interested in the absorption cross sections σ^\pm for charges of both signs. These two cross sections depend on the trajectory parameter E , as well as the background parameters α and ε . The overall charge accretion will be balanced if and only if $\sigma^+ = \sigma^-$.

Since the incoming particles are assumed to have zero initial Larmor radius, they are asymptotically locked to the magnetic field lines (which are straight lines parallel to the symmetry axis). Thus, at the limit in which the incoming particle is still far away from the BH, its motion is characterized by $r \sin \theta \rightarrow \text{const} \equiv b$ as well as $\phi \rightarrow \text{const}$, and the latter also implies $u^\phi \rightarrow 0$. Far away from the BH we also have $g_{t\phi} \rightarrow 0$ and $g_{\phi\phi} \rightarrow r^2 \sin^2 \theta \rightarrow b^2$, therefore

$$u_\phi = g_{\phi\phi} u^\phi + g_{t\phi} u^t \rightarrow b^2 u^\phi \rightarrow 0.$$

Substituting these initial far-distance limits of u_ϕ and $g_{\phi\phi}$ in Eq. (12), we obtain the relation between the impact parameter b and the conserved quantity L :

$$L = \frac{1}{2} \varepsilon b^2. \quad (13)$$

We emphasize that throughout this paper, we exclude the trivial case of $\varepsilon = 0$ from our analysis as it does not correspond to a magnetized BH.

III. TRAJECTORY SPACE

The nonlinearity of the EOM (4) and the system's non-integrable nature (due to the lack of sufficient constants of motion), imply that trajectories may display a rather complex, fractal behavior. This behavior becomes evident when numerically solving the EOM for a variety of

initial conditions (see also the discussion in Sec. VI). In particular, the set of absorbed trajectories as a function of the impact parameter b seems to be fractal, including an infinite number of absorption and non-absorption bands. This creates an inherent difficulty in the evaluation of the particle's absorption cross section. To overcome this complication, we shall seek for upper and lower bounds on the cross section (for both attracted and repelled charges), as we further explain below.

A. Trajectory types

For the purpose of investigating the cross section for absorption, it is useful to categorize particle trajectories according to their ultimate end point. This results in the definition of three different trajectory types: 1) *Falling trajectories*, which eventually cross the event horizon. For example, since the electric field along the symmetry axis vanishes ($F_{tr} = 0$), an incoming charged particle along the axis of symmetry will necessarily fall into the BH. 2) *Escaping trajectories*, that eventually go to infinity. For example, a particle with a large enough impact parameter will inevitably escape to infinity, only weakly interacting with the BH and the electric potential. 3) *Trapped trajectories*, that neither fall into the BH nor escape to infinity. For example, a particle moving in an equatorial circular orbit. The existence and categorization of such trajectories have been explored in previous studies [10–15]. In Subsec. III B we discuss another type of trapped trajectory which is of importance to the analysis of domains of accretion.

The fact that the $b = 0$ orbit is always absorbed, combined with the basic continuity of the solutions to the EOM with respect to the initial conditions, imply that in some neighborhood of $b = 0$ all trajectories are falling. On the other hand, for large enough b (with ε , E and α remaining fixed), all trajectories are obviously escaping. We accordingly define b_1 as the maximal b value up to which all trajectories are falling, and b_2 as the minimal b value beyond which all trajectories are escaping. In the range $b_1 < b < b_2$ trajectories can either fall, escape, or be trapped. We further discuss this complex behaviour (with specific regard to the fractal domain of falling orbits) in Sec. VI.

B. Critical trajectory - b_1

Since, by definition, all particles with $b < b_1$ fall into the BH, we will employ b_1 to construct a lower bound σ_{\min} on the absorption cross section, namely the area of an asymptotic disk of that radius:

$$\sigma_{\min} \equiv \pi(b_1)^2 \leq \sigma. \quad (14)$$

The trajectory with $b = b_1$ is the non-falling trajectory with minimal b (for given E , α and ε), and we will refer

to it as the *critical trajectory*.

While the definition of b_1 is simple, it turns out that the nature of this trajectory is rather subtle. Although not necessary for our analysis, we give below a brief description of some properties of this critical orbit – and how they can help pinpoint it.

The numerical determination of b_1 may be carried out quite straightforwardly by scanning along the b axis with high enough resolution until a non-falling orbit is first encountered. However, the unique properties of this orbit may be used to identify it in a more efficient way, as we now describe: Fixing E , α , and ε , we compute trajectories with gradually increasing b values starting from $b = 0$. For sufficiently small b values, all trajectories fall into the BH with negative \dot{r} throughout (outside the BH) – until one encounters the first falling trajectory where \dot{r} vanishes and subsequently changes sign at some proper time τ . We will refer to such points of sign change as *bounces*. The number of bounces steadily grows as we further increase b towards b_1 . In the limit $b \rightarrow b_1$, the number of bounces tends towards infinity – which designates the critical trajectory b_1 .

The critical trajectory $b = b_1$ itself is thus characterized by an oscillatory motion – which eventually asymptotes to a periodic orbit in both the r and θ coordinates. This also translates to an asymptotically periodic oscillatory motion in the $\rho - z$ plane, where ρ and z are cylindrical coordinates defined using the Boyer-Lindquist coordinates as

$$\rho = \sqrt{r^2 + \alpha^2} \sin \theta, \quad (15)$$

$$z = r \cos \theta. \quad (16)$$

We further elaborate on these properties of the $b = b_1$ orbit in App. A.

While for $b < b_1$ the behavior is simple in the sense that all trajectories are of the falling type, the situation is drastically different for $b > b_1$, where the set of trajectories appears to become fractal (with regards to their types). In particular, any neighborhood $b > b_1$ of b_1 , no matter how small, seems to contain both falling and escaping orbits (as well as trapped ones in between). In fact, to our understanding, within any such neighborhood, there exists an infinite sequence of alternating segments of falling and escaping orbits.

C. Universal limit of large ε

The limit of strong magnetic field for attracted charged particles, $\varepsilon \rightarrow -\infty$, is inherently, as well as astrophysically (see Sec. VI), interesting. In that limit, an attracted particle with $b > 0$ moving towards the BH will be accelerated by the electric field to ultra-relativistic velocities (as opposed to a repelled particle, that would be slowed down). Since the electric field is linear in ε , the charge will become ultra-relativistic already in the weak field region. That is, at *any* generic fixed point in space, the

four-velocity u^μ diverges like ε , hence the particle's trajectory will asymptotically tend to a light-like curve.

It is convenient to investigate this limit at the level of the EOM by reparametrizing the orbit with $\tau' = \varepsilon\tau$ instead of proper time τ , and correspondingly, defining the rescaled four-velocity $u'^\mu = \frac{dx^\mu}{d\tau'}$. Importantly, substituting these new variables in Eq. (4) yields well-behaved and effective EOM, as will be shown below. We refer to these EOM as “universal” as they are independent of both ε and E , as we will now discuss.

Under the reparametrization, the rescaled four-velocity normalization condition becomes

$$u'^\mu u'_\mu = -\frac{1}{\varepsilon^2} \xrightarrow{\varepsilon \rightarrow -\infty} 0.$$

Also, replacing $u_\mu \rightarrow \varepsilon u'_\mu$ in Eqs. (11), (12) and dividing by ε reveals that $E' = E/\varepsilon$, $L' = L/\varepsilon$ play a role analogous to that of the energy and azimuthal angular momentum in the reparametrized problem. As explained earlier, in our physical setup we fix E and investigate the orbits as a function of b , for fixed ε . Correspondingly, when we rescale the problem and take the $\varepsilon \rightarrow -\infty$ limit (with the purpose of understanding the system's behavior at strong magnetic fields), the original parameter E is kept fixed. This implies that the rescaled energy vanishes:

$$E' = 0. \quad (17)$$

For the angular momentum the situation is somewhat different: for a given impact parameter b we have $L = \frac{1}{2}\varepsilon b^2$ as seen in Eq. (13) which, when rescaled, becomes

$$L' = \frac{1}{2}b^2. \quad (18)$$

In the universal limit, therefore, there is *only one non-trivial constant of motion* L' . The fact that in this limit the dynamics of the particle are independent of the energy (and obviously ε) is the main reason behind our decision to refer to this limit as “universal”.

At the universal limit $\varepsilon \rightarrow -\infty$, the EOM take the form

$$\frac{du'^\alpha}{d\tau'} + \Gamma_{\mu\nu}^\alpha u'^\mu u'^\nu = \tilde{F}^\alpha{}_\nu u'^\nu, \quad (19)$$

combined with the null normalization condition

$$u'^\mu u'_\mu = 0, \quad (20)$$

where $\tilde{F} \equiv F/\varepsilon$ is the rescaled electromagnetic tensor, which depends only on the spin parameter α . Thus, the EOM in the universal limit portray a picture of a massless charged particle with zero energy and fixed angular momentum, moving in a magnetized Kerr background with finite field strength \tilde{F} .

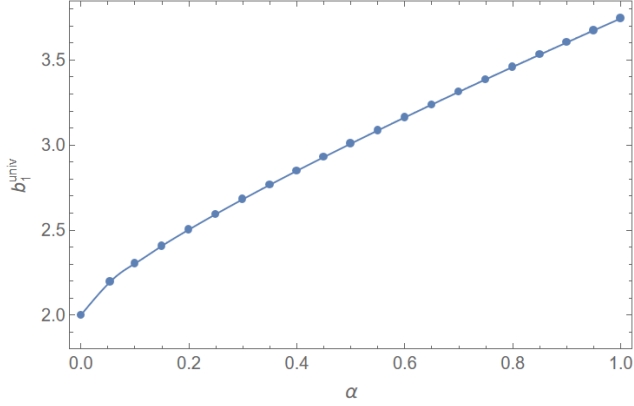


FIG. 1. The critical impact parameter b_1^{univ} in the universal limit $\varepsilon \rightarrow -\infty$, obtained numerically as a function of the spin parameter α .

While the EOM greatly simplify in the universal limit, they are still analytically intractable. Nevertheless, considering this limit enhances our understanding of the critical trajectory $b = b_1$ at $(-\varepsilon) \gg 1$. It also provides important insights on the (im)possibility of presence of the particle at any given point in space through the energy considerations described in Sec. IV in the $(-\varepsilon) \gg 1$ limit; we elaborate on this in App. C. The critical trajectory

$$b_1^{\text{univ}}(\alpha) \equiv \lim_{\varepsilon \rightarrow -\infty} b_1(\varepsilon; \alpha, E)$$

can be found numerically using the same method presented in Subsec. III B, and it presents the same qualitative behavior as described therein. Fig. 1 shows numerical results⁵ for the universal critical impact parameter b_1^{univ} as a function of spin α , computed using the universal EOM (19). As expected, for any fixed α , $b_1(\varepsilon; \alpha, E)$ converges to the corresponding critical impact parameter b_1^{univ} as $\varepsilon \rightarrow -\infty$, and this limiting parameter is E -independent. This is illustrated in Fig. 2.

IV. CONSERVED QUANTITIES BASED (CQB) CRITERION

A. Energetically allowed and forbidden regions

Instead of directly solving the EOM, one can seek an upper bound on the value of b for infalling trajectories – which, in turn, will provide an upper bound on the absorption cross section for charged particles. Here we explain how such an upper bound can be found using the particle’s constants of motion.

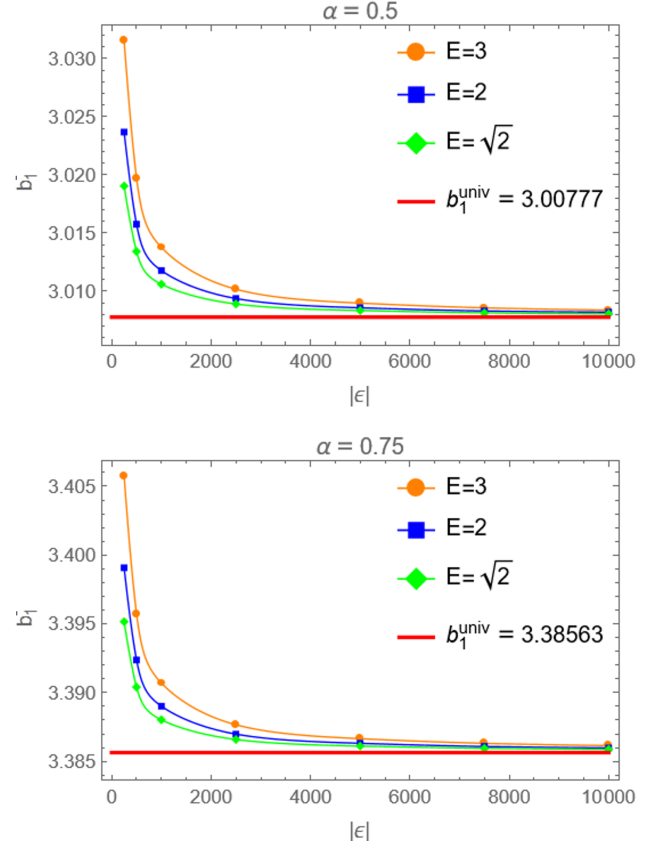


FIG. 2. Evolution of the critical impact parameter for an attracted particle, b_1^- , in the large- ε limit for three initial energies (different shapes and colors) at two values of the spin parameter α (different panels). The values of b_1^- for all initial energies converge toward the universal limit for the same α .

The timelike normalization requirement $u^\mu u_\mu = -1$ can be employed to construct a useful criterion based on the following quantity:

$$n \equiv g_{tt}(u^t)^2 + 2g_{t\phi}u^t u^\phi + g_{\phi\phi}(u^\phi)^2 + 1. \quad (21)$$

We are concerned here with the domain $r > r_+$, where both g_{rr} and $g_{\theta\theta}$ are greater than zero. Therefore, $g_{rr}(u^r)^2 + g_{\theta\theta}(u^\theta)^2$ is always non-negative, implying that n must be *non-positive* for timelike orbits. Using the conserved quantities (11),(12), we express u^t and u^ϕ as functions of r and θ :

$$\begin{aligned} u^t &= E + r \frac{2E(r^2 + \alpha^2) - b^2 \alpha \varepsilon}{\Delta \Sigma}, \\ u^\phi &= -\frac{1}{2} \varepsilon + \frac{r \alpha (2E(r^2 + \alpha^2) - b^2 \alpha \varepsilon)}{(r^2 + \alpha^2) \Delta \Sigma} \\ &\quad + \frac{b^2 \varepsilon}{2(r^2 + \alpha^2) \sin^2 \theta}. \end{aligned} \quad (22)$$

When plugged into (21), this gives us n as a function

⁵Note that in Fig. 1, as well as in Figs. 2, 6 and 7, the actual numerically calculated data are represented by points on the graphs while the curves connecting them are merely interpolations added for better visual illustration.

of r and θ :

$$n(r, \theta; b, E, \alpha, \varepsilon) = \frac{n_u}{4 \sin^2 \theta \Delta \Sigma}, \quad (23)$$

where n_u is a polynomial in all its parameters, as well as in r and $\sin^2 \theta$, which is given by:

$$\begin{aligned} n_u(r, \theta; b, E, \alpha, \varepsilon) = & b^4 \varepsilon^2 \Delta \\ & + \sin^2 \theta [4(r^2 + \alpha^2)(\Delta - E^2(r^2 + \alpha^2)) + 8b^2 E r \alpha \varepsilon] \\ & - \sin^2 \theta [b^2 \alpha^2 + 2\Delta(r^2 + \alpha^2)] b^2 \varepsilon^2 \\ & + \sin^4 \theta \Delta [4(E^2 - 1)\alpha^2 + (2b^2 \alpha^2 + (r^2 + \alpha^2)^2) \varepsilon^2] \\ & - \sin^6 \theta \varepsilon^2 \alpha^2 \Delta^2. \end{aligned} \quad (24)$$

Note that the function n depends only on the coordinates r and θ (in addition to its dependence on the system parameters α and ε , and the orbit parameters E and b). As mentioned, the particles' orbits must satisfy

$$n(r, \theta; b, E, \alpha, \varepsilon) \leq 0. \quad (25)$$

We shall refer to this inequality as the *conserved quantities based* (CQB) *criterion* (sometimes also referred to as the “energy condition” or “energy considerations” etc.).

Given fixed values of α, ε and E , our goal here is to compute an upper bound on the absorption cross section. The criterion defined in Eq. (25) allows us, for every choice of b , to divide the $r - \theta$ plane into two distinct regions: (i) The *allowed region*, defined by $n \leq 0$, is the region in which timelike trajectories can energetically be present; (ii) the *forbidden region*, defined by $n > 0$, is the region in which timelike trajectories cannot exist, as dictated by the CQB criterion. While similar methods have been used in previous studies [13, 16], to our knowledge, it has not been used to consider upper bounds on the absorption cross section of the BH for fluxes of unbound charged particles coming from infinity.

Obviously the entire trajectory of the particle must be contained in an allowed region. Therefore, for a particle to be able to fall into the BH, a connected allowed region that extends from infinity to the event horizon must exist. This implies that for this CQB analysis it is sufficient to restrict ourselves to the domain $r > r_+$. In this domain, the denominator in the right hand side of Eq. (23) is always positive (except for the case of $\theta = 0$ which will be dealt with separately below) and the sign of n is the same as that of n_u , therefore the condition in Eq. (25) reduces to

$$n_u(r, \theta; b, E, \alpha, \varepsilon) \leq 0. \quad (26)$$

Note that this criterion is mathematically more convenient than the one in Eq.(25) due to the polynomial nature of n_u .

On the axis of symmetry, namely at $\theta = 0$ (or equivalently $\theta = \pi$), the denominator of n in Eq. (23) vanishes. If $n_u > 0$ on the axis, then n diverges to $+\infty$ there, meaning that the axis and its neighborhood are forbidden in such a case. Therefore, in order for the axis and its neighborhood to be energetically allowed, Eq. (26) must hold at $\theta = 0$ as well.

B. Globally connecting and disconnecting points

Due to the vanishing of the electric potential along the symmetry axis, particles with $b = 0$ fall directly into the BH. By continuity, there exists a b -range for which all particles are absorbed into the BH. It therefore follows that for a small enough b , all b values are energetically allowed for absorption.

On the other hand, all orbits with sufficiently large b values are forbidden for absorption. To see this, note that (i) n_u is a polynomial of second order in b^2 whose coefficients are themselves polynomial in r and $\sin^2 \theta$; (ii) the coefficient of the highest order in b (namely, b^4) is $\varepsilon^2 r(r - 2) + \varepsilon^2 \alpha^2 (1 - \sin^2 \theta)$, which is always *positive* for $r > 2$. Choose now any “circle” of $r = \text{const} > 2$ and evaluate the sign of n_u on this curve. Both the coefficients of the b^2 and b^0 terms in n_u , being polynomials in $\sin^2 \theta$, are bounded from above at that r value. Since the coefficient of the highest order term b^4 is positive, it is obvious that at sufficiently large b , $n_u > 0$ is satisfied everywhere on this constant- r curve, meaning that this circle is entirely in a forbidden region. In other words, there is no allowed region connecting the horizon to infinity.

From the above, it follows that there must exist a value of b that marks a transition (with increasing b) from a b -range for which absorption is allowed to one for which it is forbidden. We call such a transition point (on the b axis) a *globally disconnecting point*. In principle, there may also exist a point of transition in the other direction (namely, from a forbidden range to an allowed one upon increasing b) which we call a *globally connecting point*.

The globally disconnecting point of largest b is of utmost importance to the question of accretion imbalance because it provides an upper bound on the accretion cross section. We denote this point by b_0 and the bound it provides on the cross section is

$$\sigma \leq \pi(b_0)^2 \equiv \sigma_{\max}. \quad (27)$$

Generally speaking, there can be two different situations:

1. There is only one globally disconnecting point (and no globally connecting points), in which case it corresponds to b_0 .
2. There are multiple globally connecting/disconnecting points, in which case b_0 will be the maximal globally disconnecting point.

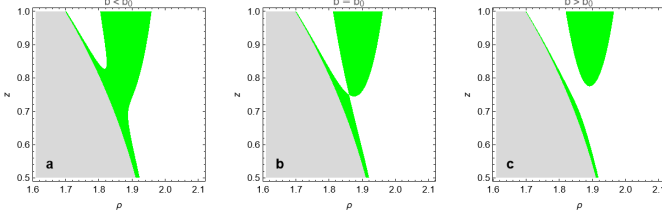


FIG. 3. Evolution with b of the allowed region for particle presence (green) for $E = \sqrt{2}$, $\alpha = 0.3$, and $\varepsilon = 10$. The (non-equatorial) critical point occurs at $b_0 = 1.87777$. The gray region represents the region $r < r_+$. Panel **a** shows the allowed region for $b < b_0$ which permits the absorption of the charged particle; panel **b** shows the disconnection of the horizon from infinity, precisely at the critical point b_0 ; and panel **c** shows the disconnected allowed regions for $b > b_0$.

We shall refer to the second case (unlike the first one) as having “energetic rings”. Each such ring may potentially provide a contribution to the absorption cross section (which nevertheless does not affect the upper bound $\pi(b_0)^2$). As we discuss later, at least in the cases considered in this paper, there actually are no such energetic rings.

C. Critical points and their classification

Finding the global connecting and disconnecting points – and most importantly b_0 – is not an easy task. In principle, one could map the allowed and forbidden regions for a dense set of individual b values, and visually extract from it the approximate b values of the globally (dis)connecting points. While straightforward, this method is computationally highly costly. As a better way for this investigation, we developed the method of *critical points*, which we here describe.

Recalling the continuity of n_u (see Eq. (24)), for fixed E , α , ε , any globally disconnecting (connecting) point that occurs at some particular b manifests itself in the $r-\theta$ plane as a point where an allowed (forbidden) region splits into two distinct regions which pinch off from each other⁶, separated by a forbidden (allowed) region; see Fig. 3 for an example of such a disconnection process at a point $b = b_0$. At each such pinch-off point, not only n_u vanishes but also its gradient must vanish, therefore, the

following set of equations must be satisfied there:

$$n_u = 0, \quad (28)$$

$$n_{u,r} = 0, \quad (29)$$

$$n_{u,\theta} = 0. \quad (30)$$

We conclude that all globally connecting and disconnecting points must correspond to solutions of this set of equations⁷. This fact provides a convenient method for finding the globally (dis)connecting points by numerically solving this set of equations. Mathematically, this set of equations typically has numerous solutions but we restrict ourselves to “physical” solutions, which are real solutions with $r > r_+$, $0 < \sin^2 \theta \leq 1$ and $b > 0$. We refer to these “physical” solutions as *critical points*^{8,9}. We empirically find that there always are at least one and at most four such critical points (for given $0 < \alpha < 1$, $E > 1$ and $\varepsilon \neq 0$)¹⁰.

Since n_u is a polynomial in $\sin^2 \theta$, any point at the equatorial plane automatically satisfies $n_{u,\theta} = 0$. Therefore, the equatorial critical points can be obtained by solving only the system of two equations $n_u = n_{u,r} = 0$ (with $\theta = \frac{\pi}{2}$) for the two unknowns r and b .

It is important to recall that not all critical points necessarily correspond to globally (dis)connecting points. That is, a (dis)connection of a certain local region does not necessarily affect the global connectivity between the horizon and infinity. Therefore, a critical point should merely be regarded as a *candidate* for a globally (dis)connecting point. Despite this subtlety, the critical points provide a very efficient method for finding the globally (dis)connecting points: as mentioned above, we found that there are only up to 4 critical points, and it is not difficult to figure out which of them are the globally (dis)connecting points. In fact, local properties of critical points provide effective information about their “global candidacy”, as we now explain.

First, a point where the gradient of n_u vanishes (as well as n_u itself) may be either (i) a local maximum/minimum or (ii) a saddle-point of n_u . Only the second case is of relevance to us, as case (i) merely represents the appearance/disappearance of an allowed/forbidden region – which does not affect the global connectivity. In other words, we are only interested here in *saddle-type* critical points. This adds the condition $\det H < 0$, where

⁷This system of equations can easily be converted to a set of *polynomial* equations in all its variables, by replacing the variable θ with $v \equiv \sin^2 \theta$ – which is more convenient for analysis.

⁸Not to be confused with the notion of “critical trajectory” which corresponds to $b = b_1$ mentioned in Subsec. III B.

⁹Interestingly, critical points can be shown to fully correspond to circular trajectories at a (not necessarily equatorial) constant θ . We hope to elaborate on this elsewhere.

¹⁰Practically, we find the critical points by solving the polynomial variant of this set of equations (see footnote 7). To this end, we use *Wolfram Mathematica*’s command *NSolve*, which solves this algebraic system easily and with any desired precision.

⁶Hypothetically, other types of (dis)connections might be possible for which at the critical b value the (dis)connection occurs along a curve in the $r-\theta$ plane rather than at a single point. However, an analytical examination (based on the *resultant* method) reveals that no such curves exist in the space of solutions.

$\det H = n_{u,rr}n_{u,\theta\theta} - (n_{u,r\theta})^2$ is the Hessian matrix determinant associated with $n_u(r, \theta)$.

The second local criterion concerns only equatorial critical points: since the θ -dependence of n_u is only through $\sin^2 \theta$, the allowed and forbidden regions have a reflection symmetry with respect to the equatorial plane. There may be equatorial critical points that merely (dis)connect allowed regions from the two sides of the equatorial plane. Such a (dis)connection has nothing to do with global connectivity between the event horizon and infinity. Therefore, we are only interested in equatorial critical points that connect two allowed regions which both have existence at the “north” (as well as the “south”) side of the equatorial plane (or in other words – a critical point that connects two *forbidden* regions from the two sides of the equatorial plane). This structure is displayed in panel **a** of Fig. 4 (unlike the situation in panel **b**). Such equatorial critical points satisfy $n_{u,rr} < 0$.

Summarizing the classification analysis above, a critical point will be referred to as a *relevant point* if it satisfies the following two inequalities:

$$\begin{aligned} \det H &< 0 \\ n_{u,rr} &< 0 \quad (\text{for equatorial points only}) \end{aligned}$$

Among the relevant points, some satisfy $n_{u,b} > 0$, which implies that two allowed regions locally disconnect as b is increased at this point in space; see Fig. 3. We refer to such relevant points as *locally disconnecting points*. Likewise, relevant points at which $n_{u,b} < 0$, will be referred to as *locally connecting points*. Any globally (dis)connecting point must in particular be a locally (dis)connecting point. Importantly, note that if there is only one locally disconnecting point, it must correspond to b_0 .

As mentioned above, in principle there might be “energetic rings”. In this case, there must be at least one globally connecting point – and also at least two globally disconnecting ones. As a matter of fact, based on the local analysis of critical points developed above, we conclude (by a combination of analytical considerations and empirical findings, which we hope to present elsewhere) that there are no locally connecting points for any point in the E and α parameter space. This of course implies that there are no globally connecting points, and thus, there are no “energetic rings”. This means that the entire domain $b < b_0$ is energetically allowed for accretion, while the entire domain $b > b_0$ is forbidden.

The scope of this paper includes an exploration of the entire ε axis (for specific values of α and E ; see Subsec. **VB**) using the critical point analysis described above. The exploration of the ε axis is done in two independent ways:

1. Applying the above mentioned critical-points classification on a dense set of ε values (for the chosen α and E).

2. Using a more analytical approach, one finds that the ε axis is divided into a certain number of non-overlapping domains (whose union covers the entire ε axis, except $\varepsilon = 0$, which is entirely excluded from our analysis), in each of which the number of critical points – and also their classification – is uniform. Each pair of adjacent domains is separated by a *transition point*, which is a certain ε value that can usually be obtained by solving a certain set of algebraic equations (which we hope to present and discuss elsewhere) for the four unknowns r, θ, b and ε . In the specific case presented in Subsec. **VB**, in the range $\varepsilon > 0$, there are four such transition points which divide the ε axis into five domains. The qualitative features derived from the local properties of the critical points, for example the lack of a local connecting point, cannot change within a particular domain. Hence, the characteristic features of the critical points within a certain ε -domain can be deduced by investigating the critical points at a single, representative, ε value in that domain. On the other hand, in the range $\varepsilon < 0$ there are no transition points – which defines the entire negative- ε range as a single domain. These conclusions (for both $\varepsilon > 0$ and $\varepsilon < 0$) are also confirmed by the search over a dense set of ε values carried out in method 1.

Using the latter method we find that in the specific case presented in Subsec. **VB** ($\alpha = 0.75, E = \sqrt{2}$), in the first four domains there is only a single locally disconnecting point – which must be b_0 . In particular, this is the situation for the specific value $\varepsilon = 2$ discussed in further details in Subsec. **VA** (this particular ε value belongs to the first domain). In the fifth domain, corresponding to ε values larger than the last transition point $\varepsilon_{\text{last}} \approx 6.8702$, there actually are two locally disconnecting points. The identification of b_0 in this case is done using a complementary analytical method as we describe in the next subsection. The implementation of the classification process for this last ε domain is demonstrated in App. **D** and compactly summarized in Table **I**.

It turns out that for sufficiently large positive ε there always is a non-equatorial critical point. In this limit, the critical point approaches the polar axis, at a limiting value $r \rightarrow r_c$ slightly larger than r_+ . The corresponding b value approaches zero as $b \approx c\varepsilon^{-\frac{1}{2}}$, where c is some positive coefficient that, like r_c , depends on E and α . The analysis of the asymptotic behavior of the set of equations (28),(29),(30) at $\varepsilon \gg 1$ – which is out of the scope of this paper – provides the values of both $r_c(\alpha, E)$ and $c(\alpha, E)$ (by solving a certain polynomial equation). A systematic check of a large dense set of α and E values indicates that there exist only a single such critical point at large ε , which always corresponds to b_0 .

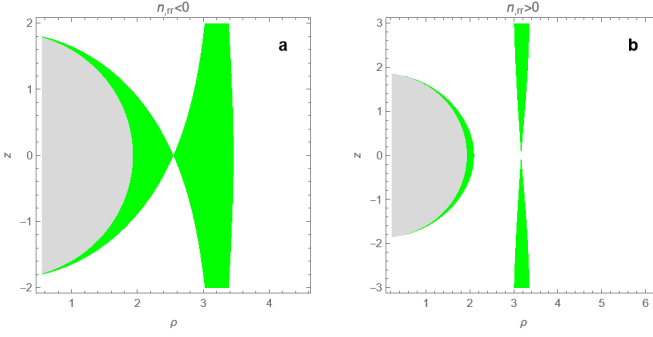


FIG. 4. Maps of allowed (green) and forbidden (white) regions for particle presence around a critical point. The gray region around the origin represents the zone $r < r_+$. In panel **a** the equatorial critical point has $n_{u,rr} < 0$ and can therefore correspond to a (dis)connection from infinity to the horizon, while in panel **b** the critical point has $n_{u,rr} > 0$ and cannot correspond to a (dis)connection from infinity to the horizon. The parameters for both panels are $E = 3$, $\alpha = 0.5$, while $\varepsilon = -100$ for panel **a** and $\varepsilon = 15$ for panel **b**.

D. An analytical upper bound

While investigating the properties of n_u we found, to our surprise, that for $\varepsilon > 0$ there exists a special value of b for which n_u vanishes on the event horizon for all θ . To show this, we substitute $r = r_+$ in Eq. (24) which yields

$$n_u(r_+, \theta) = -\sin^2 \theta [b^4 \alpha^2 \varepsilon^2 - 8b^2 E r_+ \alpha \varepsilon + 16r_+^2 E^2]. \quad (31)$$

Notice that the term in the brackets is independent of θ . Equating this expression to zero and solving for b gives a single real solution in the relevant range $b > 0$:

$$b = \sqrt{\frac{4E r_+}{\alpha \varepsilon}} \equiv b_h, \quad (32)$$

Considering first the situation at $b = b_h$, in App. B we show that at $r = r_+$, $n_{u,r} > 0$ is satisfied for all θ (including $\theta = 0$), which implies that $n_u > 0$ throughout some $r > r_+$ neighborhood of the event horizon. In other words, particles coming towards the BH with $b = b_h$ cannot be absorbed as their presence near the event horizon is forbidden. Because n_u is continuous (particularly in b), there must exist a neighborhood of $b = b_h$ throughout which the horizon is still surrounded by a forbidden region.

This fact indicates that there must exist a globally disconnecting point at $b < b_h$. Since we already showed that there are no “energetic rings”, this globally disconnecting point must be b_0 itself. Therefore, for any $\varepsilon > 0$,

$$b_0 < b_h. \quad (33)$$

As mentioned above, in the domain $\varepsilon > \varepsilon_{\text{last}}$ (for $\alpha = 0.75$, $E = \sqrt{2}$) there are two locally disconnecting points,

and we still need to find which of them corresponds to the (single) globally disconnecting point b_0 . It turns out that only the smallest of these two b values satisfies the condition in Eq. (33) – which signifies it as b_0 .

Furthermore, note that Eq. (33) in combination with Eq. (27) implies $\sigma < \pi(b_h)^2$, that is,

$$\sigma < \frac{4\pi E r_+}{\alpha \varepsilon} \equiv \sigma_h^{(+)} \quad (\varepsilon > 0). \quad (34)$$

The quantity $\sigma_h^{(+)}$ provides a powerful analytical upper bound on the accretion cross section for positive ε values – see also Subsec. V B.

V. CHARGE ACCRETION (IM)BALANCE

As explained in sections III and IV, the lower bound on the absorption cross section can be found by numerically evaluating b_1 , and the upper bound by finding b_0 – or alternatively, for repelled particles, using b_h . We implemented these methods using *Wolfram Mathematica* to compute these two bounds. Throughout this section we focus of the specific case of $\alpha = 0.75$ and $E = \sqrt{2}$. In the first subsection we specifically consider the value $|\varepsilon| = 2$ and demonstrate that charge accretion is not balanced at $Q = Q_w$. In the second subsection we extend the analysis to the entire range of ε and find that charge accretion imbalance persists for all $|\varepsilon|$ values greater than a certain, relatively small, parameter $|\varepsilon|_{\text{cross}}$ to be specified below.

The motivation for our choice of a specific ε value is simple – as even a single example of imbalance proves that the hypothesis of universal charge accretion balance at $Q = Q_w$ cannot be true. We therefore choose an explicit value ($|\varepsilon| = 2$) at which the analysis is especially simple, since it is in the domain in which there is only a single critical point. The extension of the analysis to the entire ε axis (in Subsec. V B) is motivated by our special interest in (and the special physical relevance of) the behavior of the charge accretion imbalance at large ε values.

For later convenience, we denote the absorption cross section for the attracted charge as σ^- and that of the repelled charge as σ^+ .

A. A specific example of accretion imbalance

In this subsection we focus on the specific case $|\varepsilon| = 2$ (with $E = \sqrt{2}$ and $\alpha = 0.75$). In this case, following the method described in Subsec. III B, we first find that for the attracted charge $b_1^- \approx 4.216$. Then, implementing the methods described in Sec. IV for the repelled charge, we find that at $\varepsilon = 2$ there is only a single critical point ($r_{\text{crit}} \approx 1.706$, $\theta_{\text{crit}} = \frac{\pi}{2}$, $b_{\text{crit}} \approx 2.427$). A map of the allowed and forbidden regions at $b = b_{\text{crit}}$ is presented in Fig. 5. As explained in Subsec. IV B (combined with

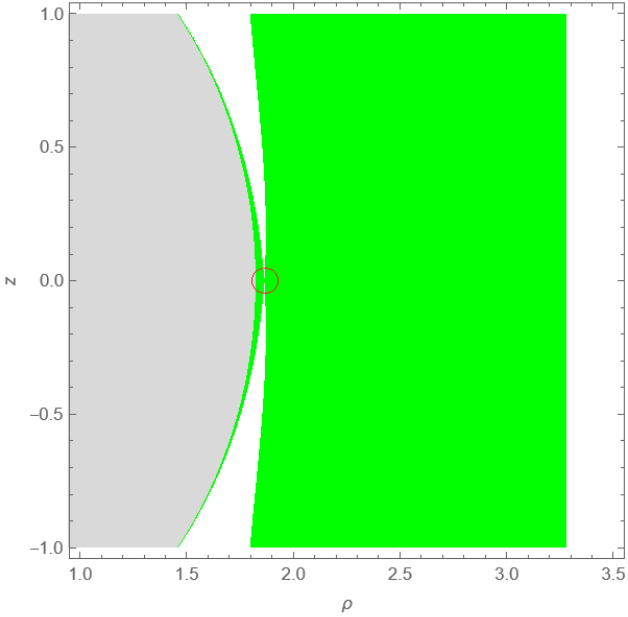


FIG. 5. Map of the allowed and forbidden regions at $b = b_0$ for $\alpha = 0.75$, $E = \sqrt{2}$ and $\varepsilon = 2$. For this choice of ε value there is only one critical point (circled in red), which necessarily corresponds to b_0 . In this case, $b_0 \approx 2.4273$.

Subsec. IV C), in such a case, b_{crit} must correspond to b_0 – namely, $b_0^+ \approx 2.427$. This is a relevant critical point (namely, it satisfies $\det H < 0$ and $n_{u,rr} < 0$) which is also locally disconnecting ($n_{u,b} > 0$) – as it should.

Implementing Eq. (14) for the attracted particle and Eq. (27) for the repelled one together with the above results for b_1^- and b_0^+ , we obtain

$$\sigma^+ \leq \pi(b_0^+)^2 < \pi(b_1^-)^2 \leq \sigma^- . \quad (35)$$

The fact that $\sigma^- > \sigma^+$ (by a significant margin – $\left(\frac{b_1^-}{b_0^+}\right)^2 \sim 3$ in this specific case) implies that at these values of E , α , and ε there is a net charge accretion imbalance in favor of the attracted charge. Therefore, Q_w cannot be the universal BH saturation charge. In the next subsection we will generalize the charge accretion analysis to the entire ε axis, demonstrating that the imbalance will actually grow with increasing $|\varepsilon|$.

B. Accretion imbalance as a function of $|\varepsilon|$

In this subsection we generalize the analysis and results presented in the previous subsection to the entire ε axis. As already mentioned above (see Subsec. IV C), to find b_0 , we carry this exploration of the ε axis using two independent methods (both yielding precisely the same results). The first one involves a dense sampling of ε values along the ε axis: we scanned the range $0 < |\varepsilon| \leq 10$ with

an increment $\Delta\varepsilon = 0.01$, and in addition, we scanned the larger range $0 < |\varepsilon| \leq 100$ with $\Delta\varepsilon = 0.1$. The second method is more analytical in nature and requires the investigation of only a single representative ε value in each of the domains composing the ε axis (see Subsec. IV C).

Although our imbalance analysis only requires b_0^+ and b_1^- , we also evaluated b_0^- and b_1^+ , and all four quantities $b_{0,1}^\pm$ are displayed as functions of ε in Fig. 6. Along with these quantities, we also display $b_h = \sqrt{\frac{4Er_+}{\alpha\varepsilon}}$ (defined for $\varepsilon > 0$) and b_1^{univ} .

As mentioned above, charge accretion imbalance is guaranteed if $b_0^+ < b_1^-$. From the behavior of these two quantities as presented in Fig. 6, we see that this inequality is indeed satisfied in the range $|\varepsilon| > |\varepsilon|_{\text{cross}} \approx 0.289$ – implying that charge accretion is imbalanced in this entire range.

The domain of large $|\varepsilon|$ is of special interest to us. In this domain, b_1^- converges to the finite (E -independent) value $b_1^{\text{univ}} > 0$ associated with the universal limit $\varepsilon \rightarrow -\infty$; see Subsec. III C and in particular Fig. 1 for b_1^{univ} as a function of α . On the other hand, as mentioned at the end of Subsec. IV C, b_0^+ decays as $c\varepsilon^{-\frac{1}{2}}$ in the limit $\varepsilon \rightarrow +\infty$. In our specific case, $\alpha = 0.75$, $E = \sqrt{2}$, we find that $c(0.75, \sqrt{2}) \approx 3.4727$. This $b_0^+ \propto \varepsilon^{-\frac{1}{2}}$ behavior can be seen in Fig. 6. Note that for this choice of parameters, we get $b_h \approx 3.53996 \cdot \varepsilon^{-\frac{1}{2}}$ which is (only slightly) larger than $b_0^+ \approx 3.4727 \cdot \varepsilon^{-\frac{1}{2}}$ – respecting the inequality in Eq. (33), as expected. In fact, at large positive ε these two curves are visually indistinguishable in Fig. 6.

We denote our upper bounds on the accretion cross sections for the two charges as $\sigma_{\text{max}}^\pm = \pi(b_0^\pm)^2$, and the corresponding lower bounds as $\sigma_{\text{min}}^\pm = \pi(b_1^\pm)^2$. The two quantities relevant to accretion imbalance, σ_{max}^+ and σ_{min}^- , are displayed in Fig. 7. This figure demonstrates that σ_{min}^- goes to a non-vanishing constant whereas σ_{max}^+ vanishes at the limit of large $|\varepsilon|$, as indeed follows from the asymptotic behavior of $b_{0,1}^\pm$ discussed above. As a consequence, the imbalance ratio $\frac{\sigma_{\text{min}}^-}{\sigma_{\text{max}}^+}$ diverges ($\propto \varepsilon$) as $|\varepsilon|$ goes to infinity.

While out of the scope of this paper, the above analysis can be performed for any desired pair of α, E . In order to explore the entire α, E plane we again proceeded in two independent methods (echoing the two methods mentioned above for exploring the ε axis): (i) We explored a dense set of points covering a large domain of the α, E plane, repeating the above mentioned analysis for each pair of α and E . (ii) We developed a more systematic methodology to identify the various *phases* in the α, E plane. These phases differ from each other in the number of transition points on the ε axis, and/or the properties of the critical points in each of the ε domains. We identified four such phases. Within each phase, the properties of the sets of critical points remain the same for all α, E pairs. All phases have several properties in common: 1. The number of critical points always lies between one and four. 2. There are no locally connecting critical points –

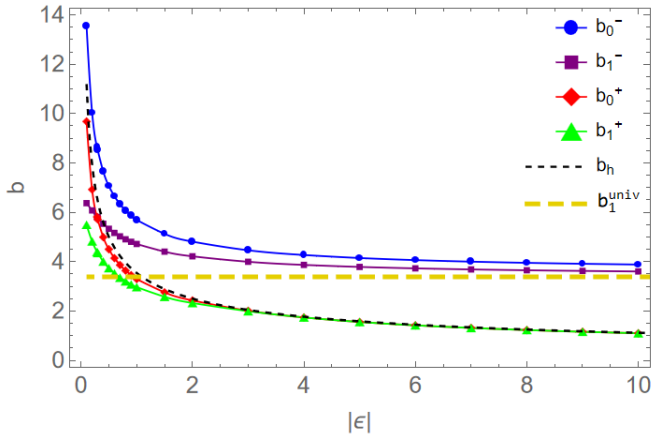


FIG. 6. The parameters b_0^\pm, b_1^\pm (which provide corresponding bounds on the absorption cross sections σ^\pm) as a function of the electromagnetic field strength parameter $|\varepsilon|$ along with the analytical curve representing b_h , and the universal $\varepsilon \rightarrow -\infty$ limit b_1^{univ} , for $E = \sqrt{2}$, $\alpha = 0.75$. The curves for b_0^+ and b_1^- intersect at $|\varepsilon|_{\text{cross}} \approx 0.289063$, above which $b_0^+ < b_1^-$, demonstrating accretion imbalance. At $\varepsilon \rightarrow \infty$, b_0^+ and b_1^+ both vanish along with b_h while the latter serves as an analytical upper bound on them. The curves for b_0^- and b_1^- converge towards different limiting values, which, for b_1^- , can be identified with b_1^{univ} .

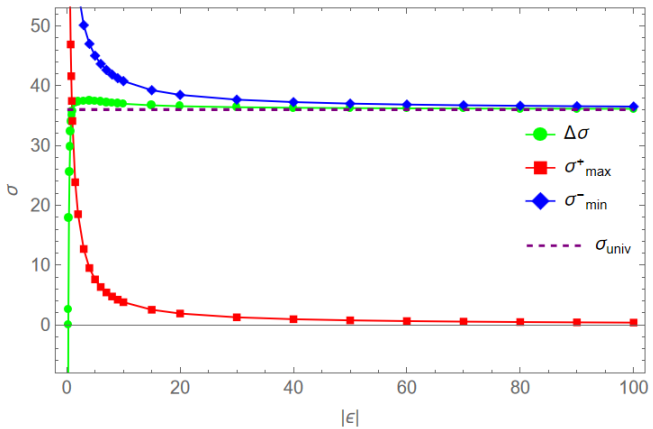


FIG. 7. The upper bound on the accretion cross section for repelled charges σ_{max}^+ , the lower bound on the accretion cross section for attracted charges σ_{min}^- , and their difference $\Delta\sigma = \sigma_{\text{min}}^- - \sigma_{\text{max}}^+$ as a function of $|\varepsilon|$, for the case $E = \sqrt{2}$, $\alpha = 0.75$. Presented as the purple dashed line is the lower bound for attracted charges obtained through the universal EOM.

which in particular implies that $b_0^+ < b_h$ is always satisfied. 3. As already mentioned above, $b_0 \propto \varepsilon^{-\frac{1}{2}}$ at large positive ε . 4. For large negative ε , $b_1^- \rightarrow b_1^{\text{univ}}(\alpha)$ (which is displayed in Fig. 1). The last two properties imply that charge accretion imbalance persists for all choices of α and E , and that the imbalance ratio diverges as $|\varepsilon| \rightarrow \infty$. We hope to further elaborate upon that extension elsewhere.

VI. DISCUSSION

In this paper we have studied charge accretion into a rotating BH embedded in an asymptotically uniform magnetic field, described by Wald's solution [1] for $A_\mu(x)$ (presented in Eq. (1)). We set the BH charge to the value proposed by Wald as the saturation charge for charged particle accretion, $Q_w = 2B_0J$. Having in mind a dilute environment where single-particle dynamics dominates, we compute upper and lower bounds on charged particles' absorption cross sections and show that at least for large enough magnetic field, the cross sections for the two types of oppositely charged particles are not equal, implying an imbalance in charge accretion at $Q = Q_w$. This is our main result, which implies that Q_w should not be thought of as the universal model-independent saturation charge: rather, the saturation charge depends on the specifics of the accretion model. This result is somewhat reminiscent of the observation made in [7], although made in a different context and system (and a different setup than the one considered by Wald), that “dynamics upstage screening”. Nevertheless, at least in an important (and likely astrophysically relevant) region of the parameter space of the model, Wald's charge Q_w still seems to provide a good approximation to the actual saturation charge, as we further discuss below.

For both positive and negative particle charge, there is a “central absorption disk” with cross sectional radius b_1 such that all orbits with $b < b_1$ fall into the BH. We solved the EOM numerically for both attracted and repelled charges and found b_1 for various choices of ε (as well as E and α) providing the *lower bound* $\pi(b_1)^2$ on the absorption cross section. We found that in the case of an attracted charge, b_1^- tends toward a constant value of order a few times M at large dimensionless field strength $|\varepsilon|$, depending only on the spin parameter α . This was found by using the $\varepsilon \rightarrow -\infty$ universal limit of the EOM introduced in Subsec. III C, where the trajectories become formally light-like and independent of E (and, obviously, of ε). This limit (which was also numerically verified; see Fig. 2) provides enhanced – yet incomplete – analytical control which improves our global understanding of the critical trajectory b_1^- . In contrast, for the repelled charge we find that for $\varepsilon \gg 1$ the corresponding critical trajectory converges towards the axis of symmetry $\rho = 0$, and in particular, the impact parameter b_1^+ decreases to zero.

On the other hand, the CQB criterion introduced in Sec. IV provides a method for obtaining *upper bounds* on the absorption cross section for charges of both signs. We use this criterion to identify spatial regions which are disallowed for the presence of the charged particle as a function of b . A particle with a given b is energetically allowed to be absorbed if and only if there is an allowed spatial region connecting the neighborhood of $\rho = b$ at large z to the horizon. By analyzing the critical points on the b axis, in which the allowed region changes its topology, we identify b_0 – namely, the maximal impact

parameter value for which absorption is energetically allowed – which provides an upper bound $\pi(b_0)^2$ on the absorption cross section. More generally, we find that the analysis of critical points (in the space of b, r and θ) provides insight into the space of possible orbits for fixed system parameters. In terms of their number and characteristics, the critical points display a rich structure which differs qualitatively in different regions of the system’s parameter space. This structure is partially discussed here, and we hope to further elaborate on it in a following paper. Finally, we show that the CQB criterion analysis significantly simplifies at $\varepsilon \gg 1$, and in particular that $b_0^+ \propto \varepsilon^{-\frac{1}{2}}$ in this regime, providing a vanishing upper bound on the cross section for repelled charges.

The accretion situation for the case of large ε therefore becomes clear: The absorption cross section of the attracted particle is bounded below by a few times M^2 , whereas that of the repelled particle vanishes as fast as ε^{-1} . This unavoidably leads to a non-vanishing net charge accretion at $Q = Q_w$. In fact, this accretion imbalance is not limited to the large- ε limit – it already occurs at ε values of order unity, as can be seen in Figs. 6, 7.

As was expanded upon in Sec. III, for $b < b_1$ all particles fall into the BH, while for $b > b_0$ particles are energetically incapable of falling into the BH. The region between these bounds, $b_1 < b < b_0$, generally shows complex behavior, and the domain on the b axis corresponding to absorption seems to be of fractal nature. This fractal behavior follows from the interplay between several basic characteristics of the system, as we hope to show elsewhere. This fractal structure is also reflected in the complex behavior of typical trajectories within this domain of b : these orbits generically bounce many times before either falling into the BH or escaping to infinity (or perhaps remaining trapped indefinitely) as demonstrated in Fig. 8. A fractal behavior of similar nature has been described in the literature in somewhat different contexts (e.g. considering different classes of orbits)[3, 7, 8].

Upon close inspection of the behavior of trajectories at $\varepsilon \rightarrow -\infty$ (using analytical as well as numerical tools), we hypothesize that in this limit all attracted particles with $b < b_0^-$ will eventually fall into the BH (except a measure-zero set), even if they bounce around in the allowed region for a long time. As a consequence, in this limit, the energetic upper bound b_0^- provides the true absorption cross section for the attracted particle: $\pi(b_0^-)^2$. We hope to expand upon this subject in the future. Since the parameter ε also depends on the charge-to-mass ratio of the particles being accreted, it is important to mention that while we assumed the same charge-to-mass ratio for attracted and repelled particles, the analysis straightforwardly generalizes to the case of different charge-to-mass ratios, and ultimately the result of accretion imbalance at Q_w is general. Namely, in a more plausible scenario involving ionized hydrogen – electrons and protons – the difference in mass will result in one of the curves (either σ_{\max}^+ or σ_{\min}^-) presented in Fig. 7 being horizontally stretched relative to the other curve (along the $|\varepsilon|$ axis).

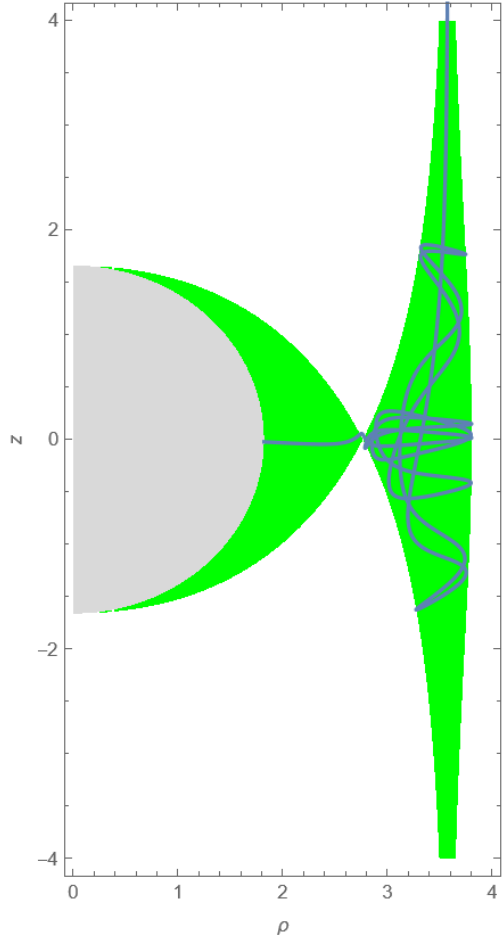


FIG. 8. The trajectory of an attracted charged particle (blue). The particle is confined to the allowed region (green), bouncing back and forth until it eventually falls into the BH. The trajectory presented here has parameters $E = \sqrt{2}$, $\alpha = 0.75$, $\varepsilon = -1000$ and $b = 3.5797444$. It has a b value very close to its corresponding b_0 .

For sufficiently large values of the asymptotic magnetic field B_0 , σ_{\max}^+ still decreases to zero proportionally to B_0^{-1} , whereas σ_{\min}^- approaches a constant of order a few times M^2 as discussed above. Therefore, accretion imbalance still occurs in this more realistic situation¹¹.

Since at the limit of large $|\varepsilon|$ the imbalance ratio diverges, one might naively expect that at this limit the actual saturation charge Q_{sat} should significantly differ from Q_w . However, a closer inspection reveals this not

¹¹When considering particles of different masses, the assumption of equal energy per unit mass E is not necessarily the most natural (e.g. when the electrons and the ions share the same temperature). Nevertheless, the vanishing of $\frac{\sigma_{\max}^+}{\sigma_{\min}^-}$ at the large- $|\varepsilon|$ limit is still guaranteed, implying accretion imbalance at $Q = Q_w$. This argument also holds for two constituents of different charge magnitudes (like fully ionized Helium).

to be the case. In a forthcoming paper [9], we will consider the correction to Q_w at large $|\varepsilon|$ within our accretion model, and show that the relative saturation charge correction $\delta \equiv (Q_{\text{sat}} - Q_w)/Q_w$ actually takes the form $\delta = \zeta|\varepsilon|^{-\frac{2}{3}}$ where $\zeta(\alpha, E)$ is an ε -independent prefactor. Thus, Q_w remains the leading-order saturation charge when $|\varepsilon| \gg 1$. To illustrate the astrophysical relevance of this regime, it is instructive to estimate $|\varepsilon|$ for electrons being accreted by Sgr A*. For this case, we can write $|\varepsilon| = \left|\frac{e}{m} B_0 M\right| \approx \frac{|e|}{m} \cdot 0.85 \cdot 10^{-20} \frac{M}{M_\odot} \frac{B_0}{\text{Gauss}}$. Plugging in the estimated BH mass $4 \cdot 10^6 M_\odot$ [17] and its surrounding magnetic field $\sim 10^2$ Gauss [18] along with the charge-to-mass ratio of the electron, we obtain $\varepsilon \sim 3 \cdot 10^9$ (and $\varepsilon \sim 10^6$ for protons).

These estimates demonstrate that the limit $|\varepsilon| \gg 1$ considered in our analysis lies well within the range expected near astrophysical BHs, motivating its physical relevance. More generally, this study offers insights into some basic mechanisms that may govern charge accumulation in rotating BHs. Such understanding may have important implications for high-energy astrophysical phenomena near BHs.

ACKNOWLEDGMENTS

We are grateful to Noa Zilberman for helpful comments. A. Ori would like to thank Bob Wald for helpful discussions. This work was supported in part by the Israel Science Foundation (grant No. 2047/23).

Appendix A: Phases of the Critical Trajectory b_1

While the critical trajectory $b = b_1$ is oscillatory for all choices of E and a , we observe that there is a critical value of ε which separates the space of critical trajectories into two qualitatively different phases, depending only on the value of ε . These two phases are characterized by an oscillation that is symmetric with respect to the equatorial plane for $\varepsilon < \varepsilon_{\text{crit}}$, and an oscillation that occurs only above the equatorial plane in the case $\varepsilon > \varepsilon_{\text{crit}}$, as can be seen in Fig. 9. It is important to note that in both phases, both the r and θ coordinates oscillate, as can be seen in Fig. 10. In the limit of $\varepsilon \rightarrow \varepsilon_{\text{crit}}$, the critical trajectory is expected to converge towards a circular orbit on the equatorial plane.

When $\varepsilon \rightarrow \infty$, the amplitude of the oscillations in both r and θ tends toward zero and b_1 approaches zero. This is because the strength of the electric potential is proportional to ε and as such, any charge coming towards the BH will be repelled well before it comes close enough to be affected by the gravitational field, except on the axis of symmetry where the electric potential vanishes.

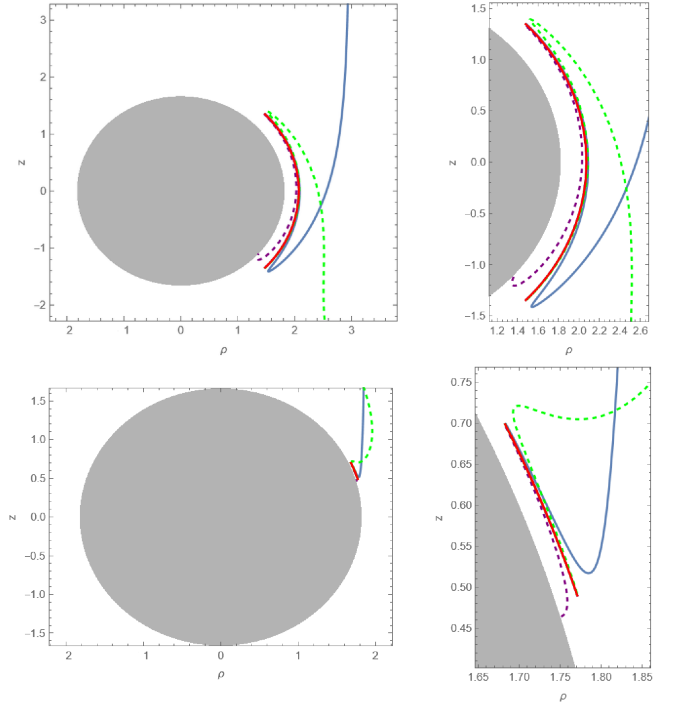


FIG. 9. The two different phases of the critical trajectory. The second column is a closeup of the first, focused on the neighborhood of the asymptotic oscillatory trajectory, further explained below. The first row represents the phase $\varepsilon < \varepsilon_{\text{crit}}$, where the critical trajectory oscillates, asymptotically symmetrically, around the equatorial plane. The second row represents the phase $\varepsilon > \varepsilon_{\text{crit}}$, where the critical trajectory oscillates without crossing the equatorial plane. The solid blue line represents the incoming critical trajectory $b = b_1$, which at late times asymptotically approaches a precisely periodic trajectory (the solid red curve). The two dashed lines show near-critical orbits coming from infinity with $b \gtrless b_1$ along trajectories very close to the blue one, which either escape to infinity (green) or fall into the BH (purple) after oscillating several times near the red curve.

Appendix B: Demonstration of $n_{,r}|_{r=r_+, b=b_h} > 0$

In this appendix we demonstrate the fact stated in Subsec. IV D, regarding the positivity of $n_{u,r}$ when evaluated at $r = r_+, b = b_h$. This implies the existence of a forbidden region surrounding the BH, which is central to justifying the use of $\pi(b_h)^2$ as an upper bound on the accretion cross section for repelled particles.

Here we will restrict ourselves to subextremal BHs, $\alpha < 1$, and moreover assume below that $\alpha > 0$ since b_h diverges at $\alpha = 0$. We denote $v \equiv \sin^2 \theta$.

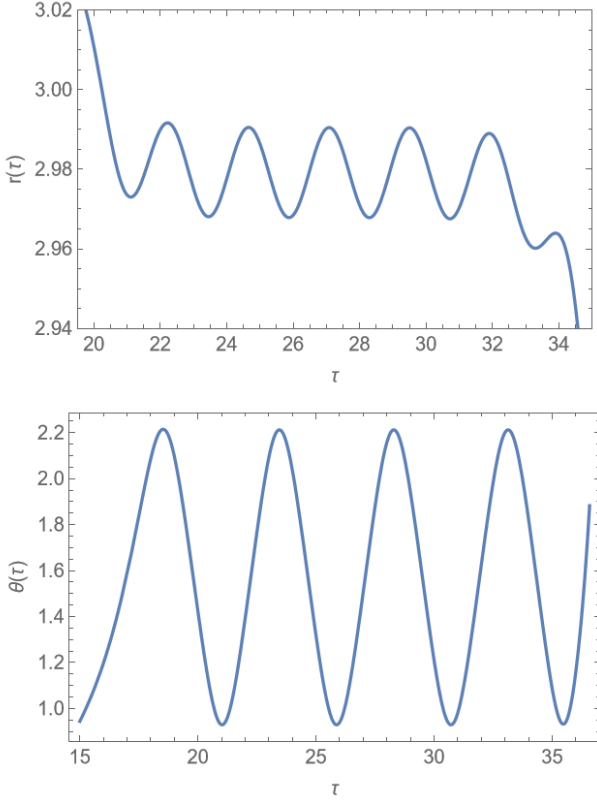


FIG. 10. Oscillations of r (top panel) and θ (bottom panel) as a function of the proper time τ . The trajectory presented here is an infalling trajectory which is very close to the critical one, with $E = \sqrt{2}$, $\alpha = 0.5$, $\varepsilon = -1$, and $b = 4.450818236305003$.

We begin by evaluating $n_{,r}$ at $r = r_+$ and $b = b_h$ (32):

$$\begin{aligned} n_{u,r}|_{r=r_+, b=b_h} &= \frac{32E^2}{\alpha^2} r_+^2 (r_+ - 1) + \frac{16v}{\alpha} r_+ (r_+ - 1) \\ &\times (-2E^2 \alpha - 2E\varepsilon r_+ + \alpha) + 8v^2 (r_+ - 1) \\ &\times (2E\varepsilon \alpha r_+ + (E^2 - 1)\alpha^2 + \varepsilon^2 r_+^2). \end{aligned} \quad (B1)$$

Our goal is to show that $n_{u,r} > 0$ for $0 \leq v \leq 1$. We first consider the boundaries of this range. At $v = 0$, we find

$$n_{u,r}|_{r=r_+, b=b_h, v=0} = \frac{32E^2}{\alpha^2} r_+^2 (r_+ - 1) > 0. \quad (B2)$$

At $v = 1$, we find

$$n_{u,r}|_{r=r_+, b=b_h, v=1} = \frac{8}{\alpha^2} r_+^2 (r_+ - 1) \left(\alpha^2 + (Er_+ - \alpha\varepsilon)^2 \right). \quad (B3)$$

This expression is clearly positive, and cannot vanish for $0 < \alpha < 1$. Therefore,

$$n_{u,r}|_{r=r_+, b=b_h, v=1} > 0. \quad (B4)$$

We have thus shown that $n_{u,r}$ is positive at the boundaries $v = 0, 1$. Now, if $n_{u,r}$ is (weakly) monotonic in the

range $0 \leq v \leq 1$, the positivity of $n_{u,r}$ follows immediately. Otherwise, since $n_{u,r}$ is a quadratic polynomial in v , it suffices to show that at its extremum, which occurs at some $0 < v_{\text{ext}} < 1$, it assumes a positive value. Solving $(n_{u,r})_{,v}|_{v_{\text{ext}}} = 0$ yields

$$v_{\text{ext}} = \frac{\alpha(2E^2 - 1)r_+ + 2Er_+^2\varepsilon}{\alpha((\alpha E + \varepsilon r_+)^2 - \alpha^2)}, \quad (B5)$$

and plugging back into $n_{u,r}$ gives

$$n_{u,r}^{\text{ext}} = \frac{8r_+^2(r_+ - 1)(4Er_+ + \varepsilon - \alpha)}{\alpha((\alpha E + \varepsilon r_+)^2 - \alpha^2)}, \quad (B6)$$

whose denominator is evidently always positive.

To complete our proof of the positivity of $n_{u,r}$, we must show that $n_{u,r}^{\text{ext}}$ is always positive when $0 < v_{\text{ext}} < 1$. By evaluating $n_{u,r}^{\text{ext}}$ at, for example, $\varepsilon = 50$, $E = 2$ and $\alpha = 0.1$, we show that there exists at least one point in the space parameterized by ε , E , and α , for which $n_{u,r}^{\text{ext}}$ is positive and $0 < v_{\text{ext}} < 1$. Let's suppose that there exists another point for which $n_{u,r}^{\text{ext}} < 0$ and $0 < v_{\text{ext}} < 1$. Since we showed that at the boundaries $v = 0, 1$, $n_{u,r} > 0$, and that the denominator of $n_{u,r}^{\text{ext}}$ is positive, by continuity there must exist values of ε , E , and α , for which $n_{u,r}^{\text{ext}} = 0$ and $0 < v_{\text{ext}} < 1$. Let us find the value of $\varepsilon = \varepsilon_0$ for which $n_{u,r}^{\text{ext}} = 0$ for any E and α . From (B6), we get

$$\varepsilon_0 = \frac{\alpha}{4Er_+}. \quad (B7)$$

Evaluating v_{ext} at ε_0 gives

$$v_{\text{ext}}^0 = \frac{8E^2 r_+}{\alpha^2(4E^2 - 1)}. \quad (B8)$$

Assuming $v_{\text{ext}}^0 < 1$, then, implies

$$E^2 < -\frac{\alpha^2}{4r_+^2}, \quad (B9)$$

and therefore no real E exists for which $v_{\text{ext}}^0 < 1$. This shows that $n_{u,r}^{\text{ext}}$ cannot vanish when $0 < v_{\text{ext}} < 1$ and, as such, $n_{u,r}^{\text{ext}} > 0$ in that case. We conclude that

$$n_{u,r}|_{r=r_+, b=b_h} > 0, \quad (B10)$$

for all α , E , ε , and $0 \leq v \leq 1$.

Appendix C: The large ε limit of b_0^-

Although not directly relevant for the main claim of this paper, here we present another application of the universal limit $\varepsilon \rightarrow -\infty$ (see Subsec. III C) – namely, the (semi-)analytical computation of the upper bound $\pi(b_0^{\text{univ}})^2$ on the large- $|\varepsilon|$ absorption cross section of an attracted particle, where $b_0^{\text{univ}} \equiv \lim_{\varepsilon \rightarrow -\infty} b_0^-(\varepsilon)$. The

CQB procedure implemented (in Sec. IV) at finite ε for finding the critical points of the normalization function n (Eq. (25)) is directly applicable to the normalization condition (Eq. (20)) associated with the universal $\varepsilon \rightarrow -\infty$ limit. It yields a set of equations analogous to Eqs. (28), (29), (30), allowing for a direct computation of the limiting value b_0^{univ} . The finite- ε values calculated for b_0^- (using the methods described in Sec. IV) show excellent convergence to this limiting value – in analogy to what was shown for b_1^- in Fig. 2.

However, we found that the value of b_0^{univ} may be obtained through a computationally simpler procedure, as we now sketch.

The normalization in the universal limit attains a remarkably simple form:

$$g^{\phi\phi}b^4 - 2b^2 + g_{\phi\phi} = 0. \quad (\text{C1})$$

When considering a particle as it crosses the equatorial plane, Eq. (C1) becomes even simpler. For any given value of $r > 2$, this polynomial in b has two real positive roots which we denote $b_{\text{root},i}(r)$ (where $i = 1, 2$). These roots then dictate the range of b values that would allow the particle to arrive at the equatorial plane at that r value. Upon further investigation one finds that the larger root, $b_{\text{root},2}(r)$, attains a minimum value at some $r \equiv r^{\min} > 2$ – which we denote $b_{\text{root},2}^{\min}$. Moreover, we find [19] that this b value actually corresponds to the maximal impact parameter for which the orbit is energetically allowed to cross the surface defined by $r = 2$ (at any θ). Consequently, every trajectory with $b > b_{\text{root},2}^{\min}$ is obviously energetically disallowed to fall into the BH (since $r_+ \leq 2$ for all α). As it turns out, $b_{\text{root},2}^{\min}$ proves to be equal to b_0^{univ} ¹². This value, which depends only on α , may be presented compactly by:

$$(b_0^{\text{univ}})^2 = \min_r \frac{r\Delta + 2\alpha\sqrt{\Delta}}{r-2}, \quad (\text{C2})$$

where, recall, $\Delta \equiv r^2 - 2r + \alpha^2$. Equation (C2) allows us to directly obtain b_0^{univ} in a simple (semi-)analytical manner.

Appendix D: An example of the classification process of critical points

We here demonstrate the implementation of our critical point classification process – and thereby the identification of b_0 – in the last ε domain (namely, $\varepsilon > \varepsilon_{\text{last}} \approx 6.8702$) for $\alpha = 0.75$, $E = \sqrt{2}$, as described in subsections IV C and IV D.

As discussed in Sec. IV, the critical points can be divided into two categories: equatorial points and non-equatorial points. For a critical point to be considered as

	$b^{(0)}$	$b^{(1)}$	$b^{(2)}$	$b^{(3)}$
Equatorial?	✗	✓	✓	✓
$\text{Sign}(\det H)$	–	–	+	–
$\text{Sign}(n_{u,rr})$	–	–	+	+
Relevance	✓	✓	✗	✗
$\text{Sign}(n_{u,b})$	+	+	+	–
Locally dis/connecting	Disconnecting	Disconnecting		
$\geq b_h$	$b < b_h$	$b > b_h$	$b > b_h$	$b > b_h$
Is b_0 ?	✓	✗	✗	✗

TABLE I. Classification of critical points in the domain of $\varepsilon > \varepsilon_{\text{last}} \approx 6.8702$ for $\alpha = 0.75$ and $E = \sqrt{2}$. The critical points are represented by their b values and in ascending order with respect to them. Each row represents a property of the critical points. The cells in gray are properties that, while remaining unchanged throughout the ε -domain, are irrelevant to the identification of b_0 . The last two points may be disqualified (for b_0 correspondence) early on as they are not relevant points. The first point is non-equatorial and therefore, the sign of $n_{u,rr}$ is irrelevant to its classification. The point which corresponds to b_0 is highlighted in green.

relevant, the sign of the determinant of the Hessian matrix of n_u evaluated at this point must be negative. Furthermore, for equatorial points, the additional condition $n_{u,rr} < 0$ must be met. After the relevant points have been identified, we seek out the points which are locally disconnecting, i.e. $n_{u,b} > 0$. Finally, to discern between remaining candidates, we identify as corresponding to b_0 the critical point whose b value is smaller than b_h .

In this domain there are only four critical points. One of them is non-equatorial, while the other three are on the equatorial plane. While their actual r, θ and b values change as a function of ε , their ordering and the properties relevant to the classification process remain unchanged throughout the entire domain. We find that for these values of α and E , the critical point corresponding to b_0 is always the single non-equatorial one. A summary of the classification process is presented in Table I.

¹²This equality reflects the fact that in the context of the universal limit, the critical point associated with b_0^{univ} is equatorial.

[1] R. M. Wald, *Phys. Rev. D* **10**, 1680 (1974).

[2] J. A. Rueda and R. Ruffini, *European Physical Journal C* **83**, 960 (2023), arXiv:2303.07760 [astro-ph.HE].

[3] J. Levin, D. J. D’Orazio, and S. Garcia-Saenz, *Phys. Rev. D* **98**, 123002 (2018).

[4] A. R. King and J. E. Pringle, *ApJ* **918**, L22 (2021), arXiv:2107.12384 [astro-ph.HE].

[5] J. A. Rueda and R. Ruffini, *European Physical Journal C* **84**, 1166 (2024), arXiv:2410.04776 [gr-qc].

[6] L.-X. Li, *Phys. Rev. D* **61**, 084033 (2000), arXiv:astro-ph/0001494 [astro-ph].

[7] P. Adari, R. Berens, and J. Levin, *Phys. Rev. D* **107**, 044055 (2023).

[8] A. M. Al Zahrani, V. P. Frolov, and A. A. Shoom, *Phys. Rev. D* **87**, 084043 (2013), arXiv:1301.4633 [gr-qc].

[9] A. Okun, E. Berreby, S. Hadar, and A. Ori, “The Saturation Charge of a Magnetized Kerr Black Hole,” (2026), in preparation.

[10] X. Sun, X. Wu, Y. Wang, C. Deng, B. Liu, and E. Liang, *Universe* **7**, 410 (2021), arXiv:2111.04900 [gr-qc].

[11] C.-Y. Liu, arXiv e-prints , arXiv:1806.09993 (2018), arXiv:1806.09993 [gr-qc].

[12] A. M. Al Zahrani, *Phys. Rev. D* **90**, 044012 (2014), arXiv:1407.7069 [gr-qc].

[13] O. Kopáček and V. Karas, *ApJ* **853**, 53 (2018), arXiv:1801.01576 [astro-ph.HE].

[14] A. N. Aliev and N. Özdemir, *MNRAS* **336**, 241 (2002), arXiv:gr-qc/0208025 [gr-qc].

[15] V. P. Frolov and A. A. Shoom, *Phys. Rev. D* **82**, 084034 (2010).

[16] K. Gupta, Y. T. A. Law, and J. Levin, *Phys. Rev. D* **104**, 084059 (2021), arXiv:2106.15010 [gr-qc].

[17] GRAVITY Collaboration *et al.*, *A&A* **677**, L10 (2023), arXiv:2307.11821 [astro-ph.GA].

[18] GRAVITY Collaboration *et al.*, *A&A* **643**, A56 (2020), arXiv:2009.01859 [astro-ph.HE].

[19] A. Okun, Master’s thesis, in preparation.